Chemosphere 340 (2023) 139855

Contents lists available at ScienceDirect

Chemosphere

journal homepage: www.elsevier.com/locate/chemosphere

Multiple phases of yttrium-doped molybdenum trioxide nanorods as efficient dye degrader and bactericidal agents with molecular docking analysis

Muhammad Ikram [a,**], Tahira Shujah [b], Anum Shahzadi [c], Ali Haider [d], Aqsa Rafique [a], Anwar Ul-Hamid [e], Walid Nabgan [f,*], Syed Karrar Haider [b], Thamraa Alshahrani [g], Mohammed M. Algaradah [h], S. Amber Yousaf [b], Junaid Haider [i]

[a] Solar Cell Applications Research Lab, Department of Physics, Government College, University Lahore, Lahore, 54000, Punjab, Pakistan
[b] Department of Physics, University of Central Punjab, Lahore, 54000, Punjab, Pakistan
[c] Facutly of Pharmacy, The University of Lahore, Lahore, Pakistan
[d] Department of Clinical Medicine, Faculty of Veterinary and Animal Sciences, Muhammad Nawaz Shareef, University of Agriculture, 66000, Multan, Punjab, Pakistan
[e] Core Research Facilities, King Fahd University of Petroleum & Minerals, Dhahran, 31261, Saudi Arabia
[f] Departament d'Enginyeria Química, Universitat Rovira I Virgili, 43007, Tarragona, Spain
[g] Department of Physics, College of Sciences, Princess Nourah bint Abdulrahman University (PNU), P.O. Box 84428, Riyadh, 11671, Saudi Arabia
[h] Chemistry Department, King Khalid Military Academy, Riyadh, 11495, Saudi Arabia
[i] Tianjin Institute of Industrial Biotechnology, Chinese Academy of Sciences, Tianjin, 300308, China

HIGHLIGHTS

- The removal of organic pollutants from water using nanomaterials was studied.
- MoO_3 and Y doped MoO_3 nanorods were prepared by co-precipitation technique.
- Significant catalytic activity was observed for 4% Y-doped MoO_3
- Y-doped MoO_3 nanorods as possible inhibitors of FabH and FabI enzymes

GRAPHICAL ABSTRACT

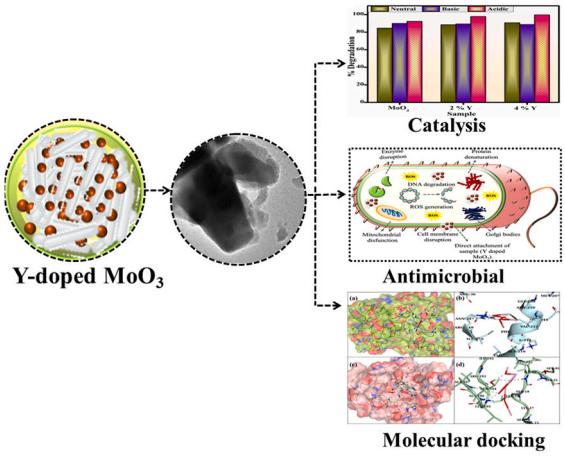

* Corresponding author.
** Corresponding author.
E-mail addresses: dr.muhammadikram@gcu.edu.pk (M. Ikram), walid.nabgan@urv.cat (W. Nabgan).

https://doi.org/10.1016/j.chemosphere.2023.139855
Received 13 March 2023; Received in revised form 15 June 2023; Accepted 15 August 2023
Available online 21 August 2023

ARTICLE INFO

Handling editor: Chang-Ping Yu

Keywords:
Co-precipitation
Methylene blue
Antimicrobial activity
Catalytic activity

ABSTRACT

Contaminants removal is usually becoming an exciting subject of research from water considering their environmental and ecological effects. This work provides pathways to remove organic pollutants from water via nanomaterials and is used as an antibiotic against bacteria like *Escherichia coli* (*E. coli*). In this study, molybdenum trioxide (MoO_3) and yttrium (Y) doped (2 and 4%) MoO_3 nanorods were synthesized by co-precipitation method. Advanced characterization techniques have been introduced to study textural structures, morphological developments, and optical characteristics of produced products. X-ray diffraction studied multiple crystalline structures of prepared samples as hexagonal, orthorhombic, and monoclinic of pure MoO_3 with decrease in crystallinity and crystallite size upon Y doping. UV–visible spectroscopy unveiled a redshift (bathochromic effect) in absorption pattern attributed to band gap energy (E_g) decreases. Photoluminescence spectra examined the recombination rate of electrons (e^-) and holes (h^+) as charge carriers. A sufficient catalytic activity (CA) was observed against methylene blue (MB) dye in an acidic medium (99.74%) and efficient bactericidal action was studied against (*E. coli)* with zone of inhibition (5.20 mm) for 4% Y-doped MoO_3. In addition, in *silico* docking demonstrated potential inhibitory effect of produced nanomaterials on FabH and FabI enzymes of fatty acid biosynthesis.

1. Introduction

The contamination of the environment has been serious, notably in air resources and water, mostly manifested in dirty water discharge by numerous businesses (Kandasamy et al., 2022). The generally identified water contaminants are organic pollutants, water-borne pathogens, heavy metals, etc. (Sharma et al., 2020). Organic dyes are widely employed in businesses and at home, for instance, in the production of clothing, leather goods, cosmetics, and plastics (Hussain and Khalid, 2022a). The pigments and dyes are fragrant and colorful organic ionizing pollutants that originate via hydrocarbons like toluene, anthracene, and xylene. The colored characteristics of dyes are attributed to auxochromes and chromophores that affect the dye solubility in solution and impart color (Gupta et al., 2013; Areerob et al., 2018; Sharma et al., 2020). According to their chemical structure, dyes can be either cationic or anionic. The reactive and acid dyes, including acid orange 7, etc., are involved in the category of anionic dye. Anionic functional groups like sulfonic or carboxylic acid are present in all cationic dyes. MB, malachite green (MG), and other dyes are classified as cationic attributed to cationic functional groups that can provide an aquatic solution with positive charge ions (Rafiq et al., 2021). Among them, methylene blue (MB), a heterocyclic aromatic chemical recognized for its dangerous effects on humans and marine life, is the most used synthetic dye. The annual discharge of MB, a carcinogenic thiazine pollutant, resulted in several environmental problems, including an increase in demand for chemical oxygen above anticipated levels that could result in the demise of marine life (Shaban et al., 2018; Din et al., 2021). Infections associated with poisoning of water resources by water-borne pathogens and dyes are major issues with water quality worldwide. To eradicate bacteria and prevent illnesses, antibacterial treatments are frequently employed in homes and hospitals (Taghizadeh et al., 2020). Numerous methods have been used to remove water contaminants, including chemical treatments, catalytic activity, degradation, coagulation, and membrane separation (Sharma et al., 2020; Naz et al., 2021). Researchers have become interested in catalysis when nanomaterial-based semiconductors are present because of the low toxicity, chemical stability, low cost, and environmentally favorable qualities of these materials (Ali et al., 2020).

In the realm of environmental remediation, such as the process of purifying water and air, semiconducting material-based catalysts have demonstrated prospective ability. Semiconductors are frequently utilized in wastewater treatment, notably for the treatment of dyes, due to their affordability, recyclable nature, low toxicity, and capacity for multiple electron transfer processes (Naik et al., 2020; Ramu et al., 2021; Kandasamy et al., 2022). When metal ions establish coordination bonds with oxides, a closely packed structure known as metal oxides is produced (Gautam et al., 2020). Several metal oxides (MOs) are used to break down various organic contaminants that exist in the industrial effluent (Vamathevan et al., 2002; Savage and Diallo, 2005; Siriwong et al., 2012); some usually acknowledged MOs include TiO_2, ZnO, SnO_2, VO_x, MoO_x, etc. (Gautam et al., 2020). Nanostructured molybdenum trioxide (MoO_3), a transition metal oxide semiconductor (TMOS), has drawn interest because of its versatile optical, structural, and electronic properties. Its improved intercalation chemistry also has special chemical and catalytic characteristics making it a potential candidate for antibacterial agents (Sen et al., 2019). Many organic compounds have antibacterial properties, however the majority of them are poisonous by nature. Under great stability and non-toxic nature, metal oxide nanoparticles have been in increasing demand in recent years as antibacterial agent. MoO_3's toxicity to pathogenic microorganisms has been investigated by K. Krishnamoorthy et al. (2013). According to this paper, when tested against the 4 bacterial species, *E. coli*, B. Subtilis, S. Typhimurium and E. Faecalis, produced MoO_3 nanoplates demonstrate good antibacterial activity (Magaldi et al., 2004; Desai et al., 2015; He et al., 2022, 2023). N. Rajiv Chandar et al. produced MoO_3 NPs via wet chemical method and studied antibacterial behavior against (*E. Coli*) and (*S. aureus*) bacteria (Valgas et al., 2007; Rajiv Chandar et al., 2021). MoO_3 is an n-type semiconductor having large indirect E_g 3.87 eV exist in three different crystallographic forms: hexagonal (h–MoO_3), orthorhombic (α–MoO_3) and monoclinic (β–MoO_3) (Raj et al., 2022; Sharma et al., 2022). The monoclinic and hexagonal phases are metastable, while orthorhombic is a thermodynamically stable phase (Dewangan et al., 2022).

The researchers have prepared MoO_3 along unique morphologies as nanobelt arrays, nanobelts, nanotubes, and nanorods using numerous synthesis techniques involving thermal evaporation, chemical vapor deposition (CVD), and chemical synthesis method (Donnadieu et al., 1988; Senthilkumar et al., 2016; Hussain and Khalid, 2022a). The cost-effective and eco-friendly co-precipitation technique allows for changes to the particle shape, surface area, and size distribution (Calderón et al., 2020). The conditions for the reaction, including the starting materials, solvent, temperature, and reaction time, are often tuned to control the shape and size (Dewangan et al., 2022). The performance of a material can be significantly affected by changing the properties of semiconducting material via doping, composition, and hybrid creation (Kandasamy et al., 2022). Rare-earth metal ion doping can decrease the E_g, providing an improved pathway for the steady flow of electron-hole pairs (Chahal et al., 2019). The surface segregation of Y^{3+} ions produces many oxygen vacancies, making a rare earth element, yttrium (Y), a useful dopant (Parangusan et al., 2018). The present work reveals a co-precipitation method for synthesizing MoO_3 nanorods and yttrium (2 and 4%) doped MoO_3 nanorods. To degrade MB from an aqueous solution, the prepared products were utilized as a catalyst. The agar well diffusion method was introduced to test synthesized samples' ability to kill bacteria like *E. coli*.

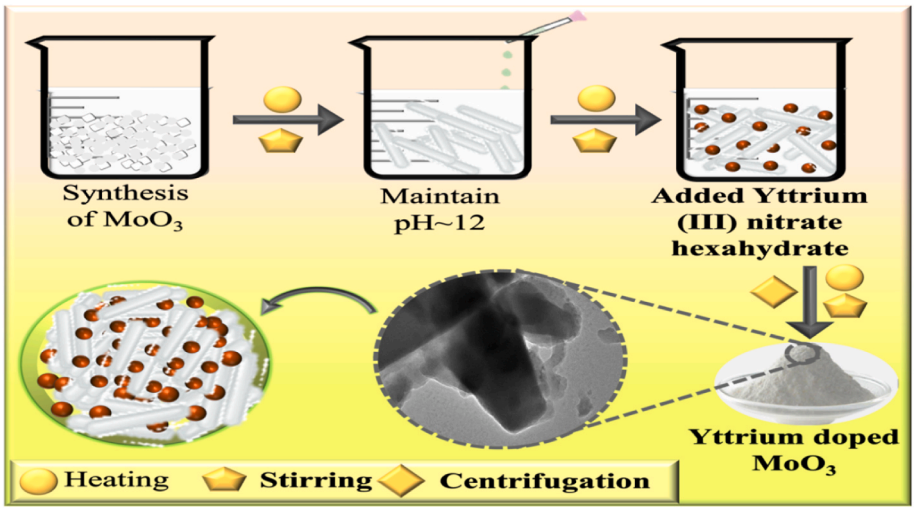

Fig. 1. Schematic illustration of Y-doped MoO_3.

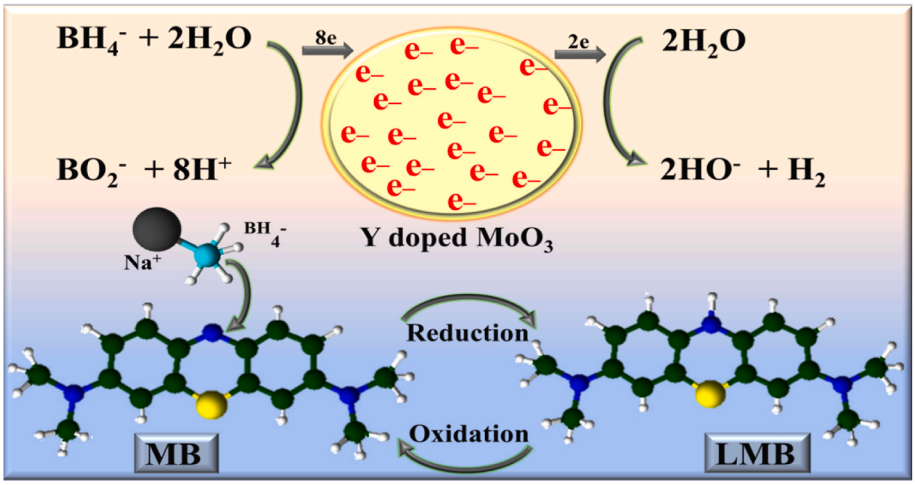

Fig. 2. Catalysis mechanism during Y-doped MoO_3 catalyst.

2. Experimental section

2.1. Materials

Yttrium (III) nitrate hexahydrate ($Y(NO_3)_3$. $6H_2O$) 99.8% and ammonium molybdate $(NH_4)_6Mo_7O_{24}.4H_2O$ were purchased from Sigma Aldrich. The nitric acid (HNO_3) brought from Merck.

2.2. Synthesis of Y-doped MoO_3

0.3 M of $(NH_4)_6Mo_7O_{24}.4H_2O$ was synthesized under magnetic stirring for 40 min at 70 °C. HNO_3 was incorporated in the continuously stirring transparent solution to convert it into a colloidal solution by maintaining pH of up to 1. The prepared precipitates were centrifuged at 7500 rpm twice to detach unwanted material and washed precipitates were dried at 120 °C for 12 h. The final product was ground to fine powder. The same process was followed to prepare doped samples of concentrations of 2% and 4% of ($Y(NO_3)_3.6H_20$), as depicted in Fig. 1.

2.3. Catalysis

To study catalyst role during water cleaning process, CA was performed in the absence of light against organic pollutant (MB) at various pH levels, in existence of a reducing agent ($NaBH_4$). Acidic and basic media were obtained by adding H_2SO_4 and NaOH, respectively. $NaBH_4$ solution was obtained by adding sodium borohydride ($NaBH_4$) into water. The prepared $NaBH_4$ (400 μL) was incorporated into 3 mL aqueous MB solution and the degradation rate was measured using (eq. (1)). After that, 400 μL of pure and differing concentrations of Y-doped MoO_3 was added to the above solution (containing MB and reducing agent). Decolorizing the solution identifies dye degradation, resulting in MB reduction into the leucomethylene blue (LMB). The experiment was performed at room temperature and prepared products were analyzed using a UV–Vis spectrophotometer. Percentage degradation was calculated via formula:

$$\% \text{ Degradation} = (C_o\text{-}C_t/C_o) \text{ x } 100 \quad (1)$$

Where C_o and C_t are dye concentrations at initial and degradation times.

2.3.1. Catalysis mechanism

In the catalysis mechanism, nano-catalysts and reducing agents ($NaBH_4$) are major components considered necessary for the degradation of organic pollutants (MB), as shown in Fig. 2. At the start, $NaBH_4$, which acts as a reducing agent, and MB, which acts as oxidizing agent, react with each other, and the rate of reaction is very slow in the absence of a nano-catalyst. The reaction rate enhanced after the addition of catalyst (MoO_3 and Y-doped MoO_3) by reducing activation energy

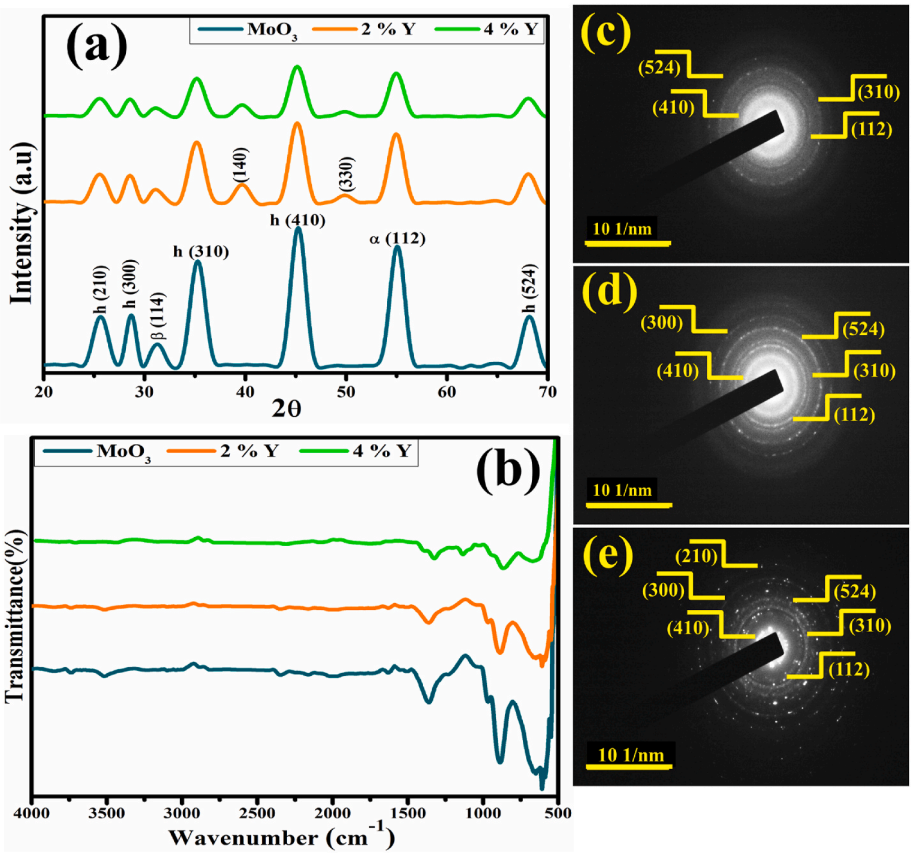

Fig. 3. (a) X-ray diffraction patterns, and (b–d) SAED patterns of pure and Y (2%, 4%)-doped MoO_3 nanorods.

required for reaction start and further preceded reaction quickly. The catalyst works as an electron relay amongst species of reactant and product, making easier the electron (e^-) transfer from BH_4^- that acts as a donor to (MB) accepter. The $NaBH_4$ and nanocatalyst presence enhanced the degradation efficiency, demonstrating that during MB reduction, $NaBH_4$ does not work as a catalyst. The catalyst amount utilized in this degradation reaction is crucial because as the catalyst amount grows, so does the degree of dye degradation (Naz et al., 2021; Raza et al., 2021).

2.4. Isolation and identification of MDR E. coli isolation of E. coli

2.4.1. Sample collection

Selected lactating cows were offered for sale in Punjab, Pakistan, at several marketplaces, veterinary offices, and farms. Direct milking of cows into sterile glassware produced samples of camelus milk. After being collected at 4 °C, raw milk was quickly brought to lab. On MacConkey agar, coliforms found in raw milk were counted. At 37 °C, the plates were incubated for 48 h.

2.4.2. Identification and characterization of bacterial isolates

Preliminary identification of (*E. coli)* was based on colonial morphology by Gram stain and by various biochemical tests with reference to Bergey's Manual of Determinative Bacteriology (Bergey, 1994).

2.4.3. Antibiotic susceptibility

The antibiotic susceptibility test was completed via disk diffusion method of Bauer et al. (1966) on 1 (MHA). The test was done to identify the antibiotic resistance of (*E. coli)* against the following antibiotics (classes); 2 (Cro) 30 μg (Cephalosporins), 3 (Gm) 10 μg (Aminoglycosides), 4 (Cip) 5 μg (Quinolones), 5 (Te) 30 μg (Tetracyclines), 5 (Imi) 10 μg (Carbapenem), 6 (A) 30 μg (Penicillins), and 7 (Azm) 15 μg (Macrolides) (Adzitey et al., 2022). Purified cultures of *E. coli* were grown and adjusted to 0.5 MacFarland turbidity. Then it was spread plated on (MHA) (Oxoid Limited, Basingstoke, UK), and the antibiotic disks were placed on inoculated plate surfaces at a distance to avoid the overlapping of inhibition zones. Plates were incubated at 37 °C for 24 h, and the outcomes were interpreted according to the Clinical and Laboratory Standard Institute (Clinical, Institute, L.S., 2017). Bacterium found resistant to minimum of three antibiotics was declared MDR (Iwalokun et al., 2004). Where 1, 2, 3, 4, 5, 6 and 7 written for Mueller Hinton agar, Ceftriaxone, Gentamicin, Ciprofloxacin, Tetracycline, Imipenem, Amoxycillin and Azithromycin respectively.

2.4.4. Antimicrobial activity

In vitro antimicrobial potential of MoO_3, Y (2 and 4%) doped MoO_3 nanorods were studied by agar well diffusion method upon ten representative isolates of MDR *E. coli* collected from mastitic milk. Petri dishes were swabbed with 1.5×10^8 CFU/mL (0.5 McFarland standard) MDR *E. coli* on MacConkey agar. Wells of 6 mm diameter were generated via sterile cork borer. Various concentrations of MoO_3, Y (2 and 4%) doped MoO_3 nanorods were applied as (0.5 mg/50 μL) and (1.0 mg/50 μL). Ciprofloxacin (0.005 mg/50 μL) was used as the positive control and DI water as the negative control (50 μL) (Haider et al., 2020b).

2.4.5. Statistical analysis

The antimicrobial efficacy was measured in terms of inhibition zone (mm) size, and inhibition zone diameters were calculated statistically by one-way analysis of variance (ANOVA) using SPSS 20 (Haider et al., 2020a).

2.4.5.1. Molecular docking analysis. Molecular docking was conducted against specific enzyme targets pertaining to fatty acid biosynthesis pathways, namely enoyl-[acyl-carrier-protein] reductase (FabI) and

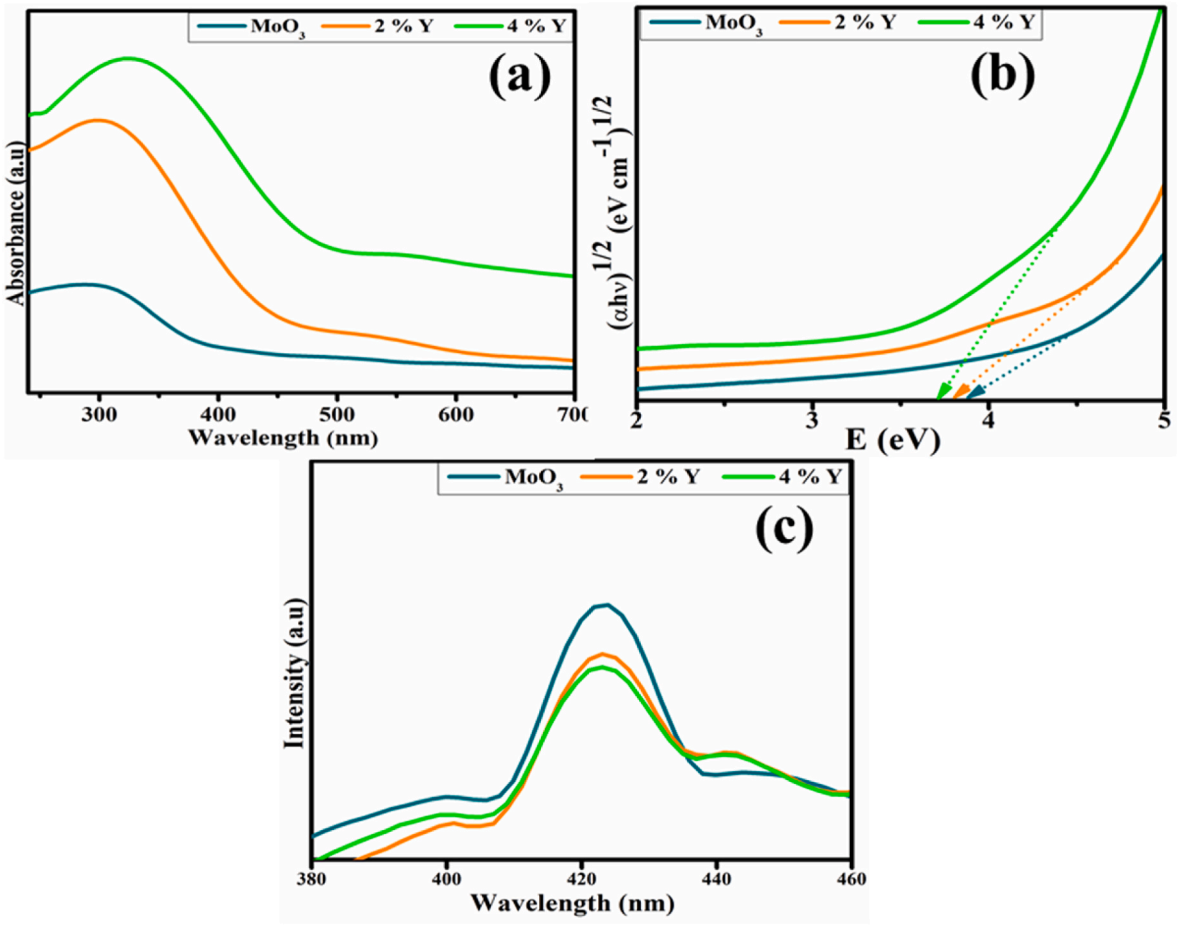

Fig. 4. (a) Absorbance spectra, (b) Eg graph, and (c) PL spectra of the MoO_3 and Y (2%, 4%)-doped MoO_3 nanorods.

β-ketoacyl acyl carrier protein synthase III (FabH) from *E. coli*. FabH (PDB ID: 5BNM; Resolution: 1.7 Å) (McKinney et al., 2016) and FabI (PDB ID: 1MFP; Resolution: 2.33 Å) (Seefeld et al., 2003) 3D conformations were retrieved from Protein Data Bank using corresponding PDB IDs. Sybyl X-2.0 (Mehmood et al., 2022) was used to predict molecular docking, using ligand structures built by sketch module. The water molecules with native ligands were eliminated, polar H-atoms were added to each molecule, and energy was then conserved. The binding pocket was defined to be within 5 of the endogenous ligand. In each scenario, the top 10 docked complexes were formed and chosen for subsequent study. Pymol software was used to build a 3D representation of binding interactions.

2.5. Characterization techniques

Powder XRD with range of 10°–60° was used to determine the structural and crystallographic behaviors of the produced powder. To find functional groups in Y (2 and 4 wt %) doped MoO_3 nanorods, FTIR spectroscopy was conducted between 4000 and 400 cm^{-1}. Through the use of EDS, SEM, and HR-TEM, the chemical makeup, surface analysis, morphology, and d-spacing of Y (2%, 4%) doped MoO_3 nanorods were all examined. To verify the produced samples' crystallinity, SAED analysis was also carried out. The optical characteristics were assessed using a Genesys 10 S UV–vis spectrophotometer, and the electron-hole recombination in the synthesized sample was examined using PL spectroscopy.

3. Result and discussion

The pure and doped MoO_3 samples' phase, crystallinity, and crystal structure were analyzed via XRD ranging from 20° to 70° as illustrated in Fig. 3(a). The peaks observed at 25.80°, 29.35°, 35.45°, 45.47° and 68.88° corresponding to MoO_3 hexagonal phase referred to as planes (210), (300), (310), (410) and (524) that well matched with standard data (JCPDS card no.00-021-0569). The pure sample also exhibited orthorhombic crystal structure with diffraction peak at 55.78° indexed to the planes (112) according to (JCPDS card no.01-075-0912). The monoclinic Mo_9O_{26} diffraction peak was observed at 31.93° (114) evidenced by (JCPDS card no.03-065-1292). Upon Y (2 and 4%) doping, some diffraction peaks were obtained for $Mo_4O_{15}Y_2$ at 39.97°, and 50.45° corresponds to diffraction planes (140) and (330) matched with (JCPDS card no.00-053-0358). Additionally, it has been found that peak positions of MoO_3 nanorods doped with rare earth element Y have a slight shifting toward the lower angle. The dopant and host material ionic radii as well as oxidation states are highly implicated in this shift. As a result, the MoO_3 lattice experiences structural strain attributed to dopant with the greater ionic radius. The insertion of imported Y-atoms into pure material lattice results in tensile stress, which causes structural strain. As an outcome, MoO_3 lattice is stretched upon doping, and peaks move towards lesser 2θ (Al-Otaibi, 2021). The transmission spectra of infrared radiation was studied using the FTIR technique to characterize vibrations of different molecules in prepared samples. MoO_3 and Y (2 and 4 wt %) doped MoO_3 nanorods' vibrational spectra in the 4000-500 cm^{-1} wavenumber region are depicted in Fig. 3(b). The band at 2359 cm^{-1} was attributed to H–O–H bending mode of water and band vibrations at 1384 cm^{-1} were detected due to vibration mode of Mo–OH

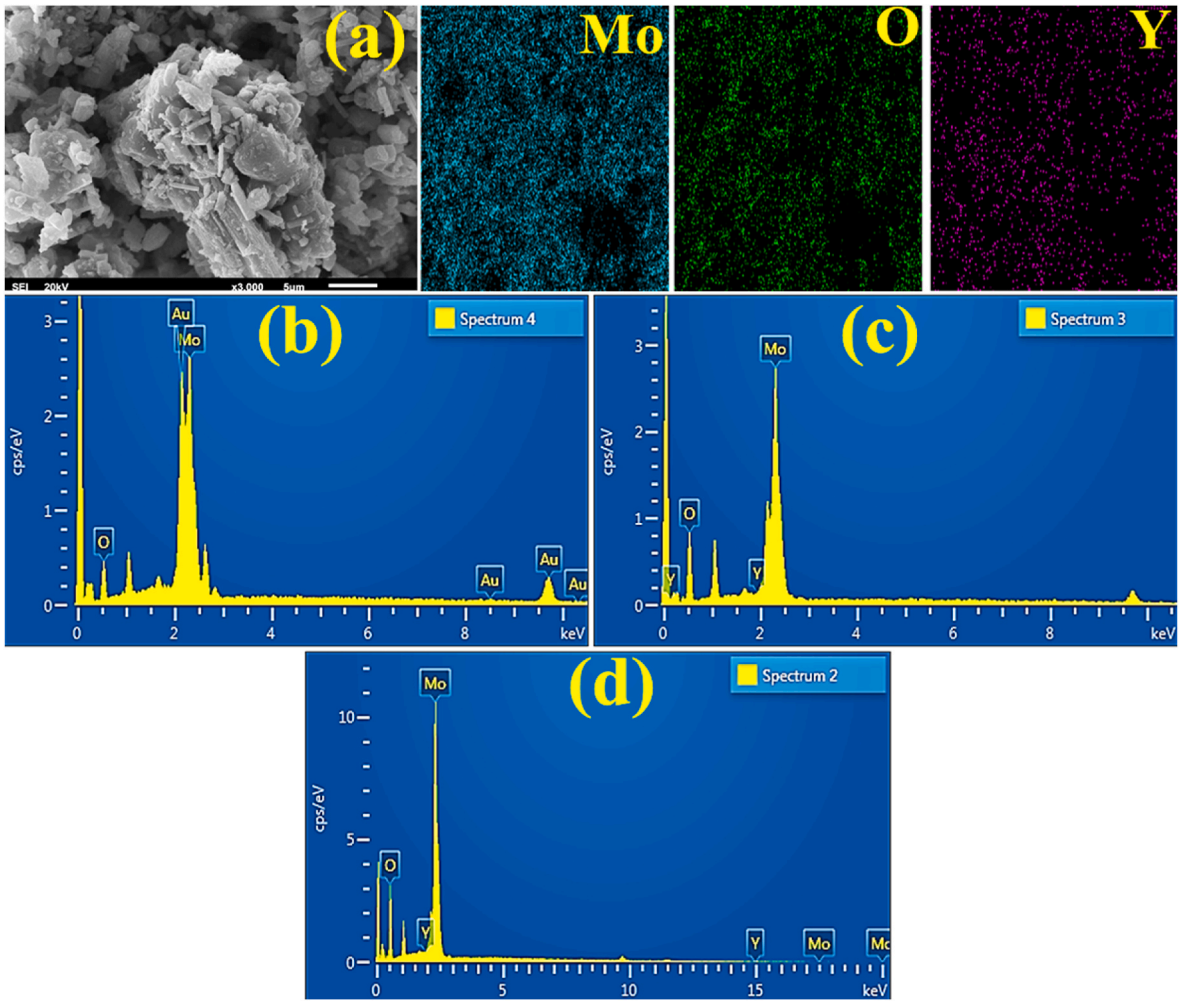

Fig. 5. (a) EDS Mapping of pure sample and identified elements (Mo, O, and Y) and (b–d) EDS patterns of pure and Y (2 and 4 wt %) doped products.

bond (Lippincott, 1963; Zakharova et al., 2007; Klinbumrung et al., 2012). At 990 cm^{-1} and 871 cm^{-1}, strong vibration bands corresponding to the stretching vibrations of Mo=O are seen. A strong peak at 605 cm^{-1} was attributed to the stretching vibrations in the Mo–*O*–Mo units of oxygen atoms (Irmawati and Shafizah, 2009; Gowtham et al., 2018). Moreover, SAED analysis shows intense circular rings of MoO_3 and Y–MoO_3 nanorods, as shown in Fig. 3(c–e), indicating the specimens are extremely crystalline. Bragg's diffraction-compliant XRD results were highly associated with different nanorods planes.

To explore optical properties in the range of 200–500 nm, a UV–vis spectrophotometer was used. The optical absorption of MoO_3 defines a typical absorption peak at 320 nm, and E_g was predicted to be around 3.87 eV for the undoped product MoO_3, since it is an indirect band gap material matched with the literature well (Sharma et al., 2022), Fig. 4 (a). The absorption intensity is primarily determined by particle size, carrier concentration, and the surrounding medium dielectric properties (Bhargava and Khan, 2017). The optical transition was between the oxygen atoms' lone pair of electrons in their "p" orbitals (O^{2-}) and vacant "d" orbitals of cation (Mo^{6+}) (Yogananda et al., 2018). Upon doping with Y (2 and 4%), the absorption shifted towards higher wavelength, ascribed to decrease in Eg. The Eg values were measured as 3.87, 3.83, 3.79 for MoO_3 and (2%, 4%) Y-doped MoO_3 nanorods using Tauc's equation, as represented in Fig. 4 (b).

As PL emission proceeds from the free carriers recombination either directly (band-band) or indirectly by band gap state, it may be utilized to examine effectiveness of charge carrier trapping, transfer and to determine the destiny of e^- and hole h^+ pairs in semiconductor (M et al., 2016). The excitation wavelength was taken at 245 nm, PL graph for pure and doped MoO_3 nanorods were examined from 380 to 460 nm to analyze the recombination rate and changes in the electron transfer efficiency as depicted in Fig. 4 (c). Emission spectra examined the peak at 424 nm for MoO_3 nanorods (Hussain and Khalid, 2022b). Surface flaws like Mo or oxygen vacancies caused the emission peaks in the 380–460 nm range. Bond breakage and surface tension brought on by a higher surface-to-volume ratio caused imperfections in MoO_3 (Yogananda et al., 2018). The large defects and high exciton recombination rate that result from Y doping cause the intensity of doped samples to rise. Additionally, the emission spectra were somewhat pushed towards longer wavelengths.

To study further interfacial contact, EDS mapping of undoped samples was done to examine the elemental distributions displayed as distinct colors. Three elements (Mo, O, Y) were studied with different compositions, as illustrated in Fig. 5 (a). The chemical composition of prepared products was studied via EDS spectra, as presented in Fig. 5 (b–d). Noticeable peaks of Mo with O unveil the successfully prepared MoO_3 nanostructures Fig. 5 (a), whereas the Au peak emerged, which was attributed to some contaminants and the gold coating applied on top of the sample. The presence of Y in doped samples spectra successfully confirms dopant incorporation, as shown in Fig. 5 (b, c).

TEM analysis was utilized to study the interior morphology of MoO_3 nanostructures. The rod-like structures with small-size particles were examined for pure MoO_3 nanostructures, as illustrated in Fig. 6 (a). Upon Y (2 and 4 wt %) doping, as presented in Fig. 6 (b, c), the highly agglomerated rods-like shapes along particles were observed forming a

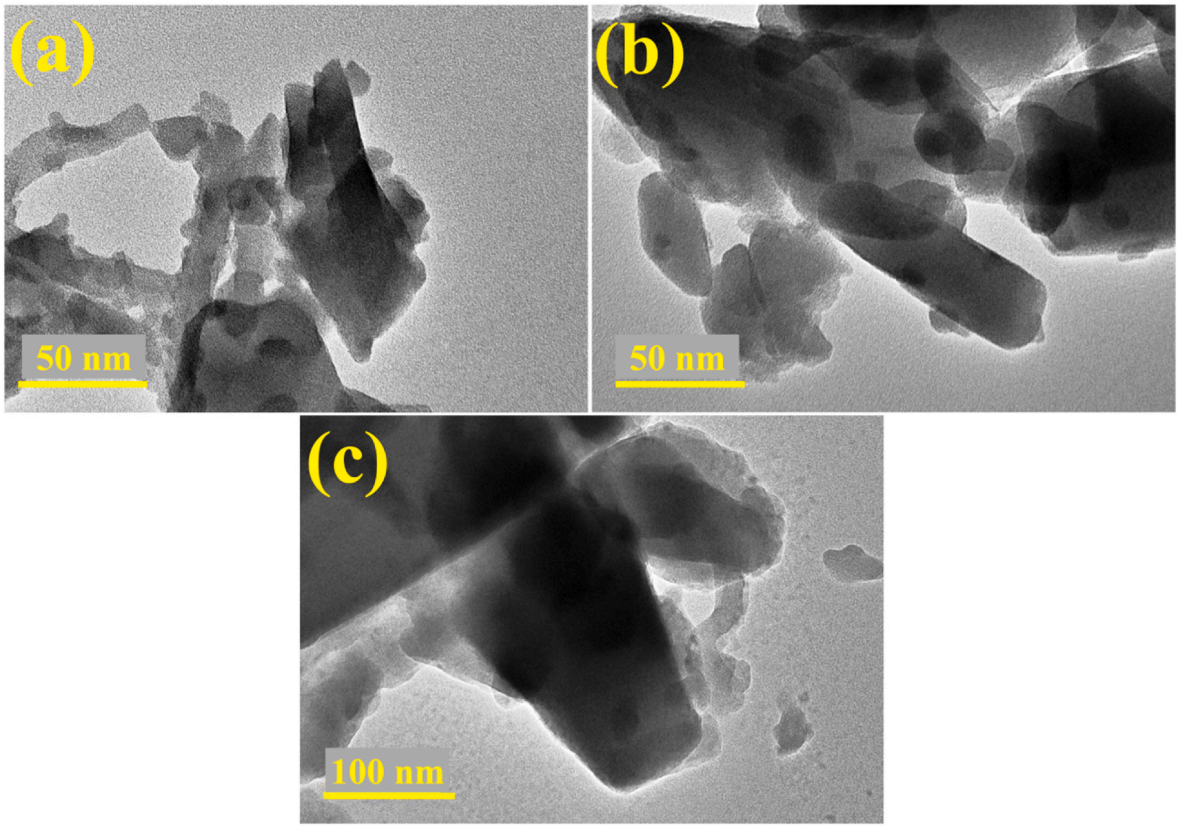

Fig. 6. (a–c) TEM image of MoO_3 and Y (2%, 4%)-doped MoO_3 nanorods.

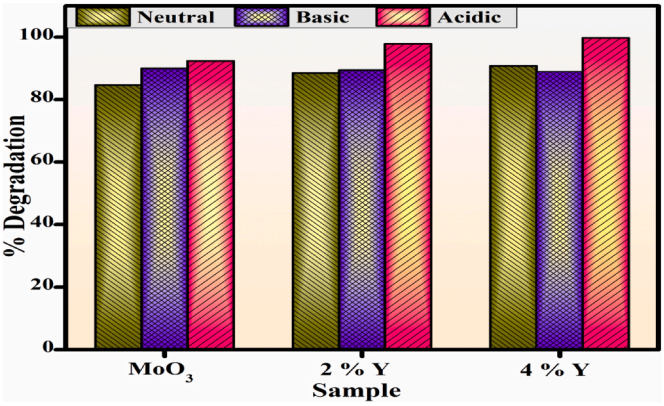

Fig. 7. Catalytic activity of pure and Y (2 and 4%) doped MoO_3 nanorods in neutral, basic, and acidic medium.

chain-like pattern; also, the size of nanostructures enhanced with the addition of Y.

The CA of pure and Y (2 and 4 wt%)-doped MoO_3 nanorods along $NaBH_4$ as reducing agent for degradation of MB in neutral, basic and acidic media were studied by UV–vis spectrophotometer. Dye waste is regularly discharged at different pH; the degradation rate is regulated by pH solution, and influences manufactured catalysts. The pure and doped MoO_3 nanorods exhibited maximum degradation of 84.61%, 88.54%, and 90.78% in neutral (pH = 7), 90.0%, 89.39%, and 88.93% in basic (pH = 10), and 92.38%, 97.87% and 99.74% in acidic (pH = 4) media (Fig. 7). 4% Y-doped MoO_3 nanorods explored the maximum catalytic activity against MB dye in an acidic medium. Even though the basic medium is deficient in H^+ atoms, hydroxyl (OH^-) ions excess attributed to NaOH stick to surface of catalyst and causes a full negative charge

Table 1
Antibacterial activity of MoO_3 and Y (2 and 4%)-doped MoO_3 nanorods for MDR *E. coli*.

Samples	Low concentration (0.5 mg/50 μL)	High concentration (1.0 mg/50 μL)	Control positive (mm)	Control negative (mm)
MoO_3	2.65	4.05	4.45	0
2% Y-doped MoO_3	2.35	4.75	5	0
4% Y-doped MoO_3	3.45	5.20	5	0

there. The hydrogen ions (H^+) generation, which causes the catalyst surface to become positively charged more, is directly related to CA in an acidic media. The H_2SO_4 existence, which contributes to MB reduction into LMB, is the reason for increased CA in an acidic medium. The 4% Y-doped MoO_3 nanorods revealed excellent CA in an acidic medium, providing the best catalyst for dye degradation. As in obtained results of the experiments, acidic environments showed the highest dye degradation value. The rate of reactions is accelerated by the particle's huge surface area and small size (Hassan et al., 2020; Qumar et al., 2020; Ikram et al., 2021).

It is crucial economically to look at the nano-catalyst's stability. The Y (4%) doped MoO_3 nanorods produce outstanding dye degradation results. In order to determine, the dye reduction in the presence of the nanocatalyst is stable or not, the stability of the catalyst at different pH (7, 10 and 4) was studied by allowing the experiment to run for at least 72 h. As illustrated in Fig. S1, the degradation was tracked after 24 h using absorption spectra collected by a UV–vis spectrophotometer while the deteriorated dye was stored in the dark. The acquired findings show that under uniform conditions for 72 h, no loss of degradation took

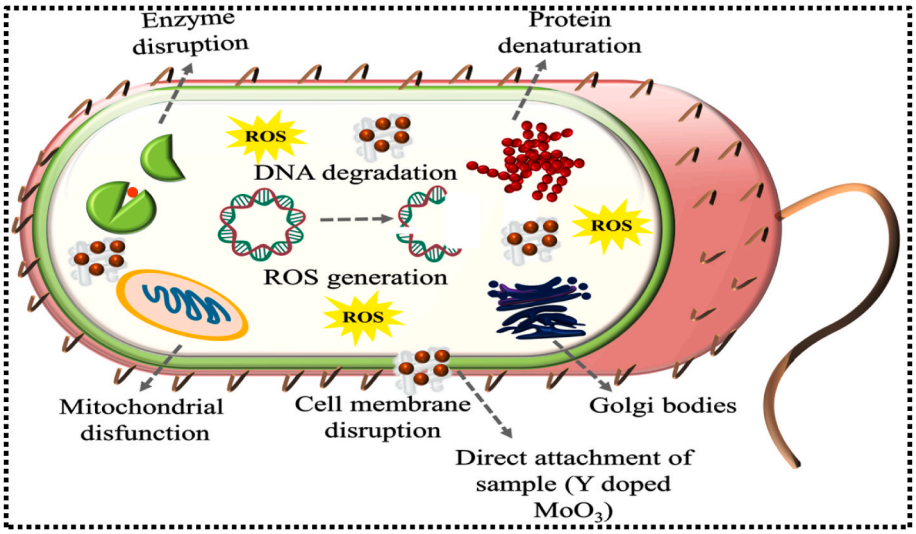

Fig. 8. Mechanism behind the antimicrobial activity of Y-doped MoO_3.

place. Degradation was seen to be in its original state, which supports the catalyst's stability.

In vitro antimicrobial activity of pure and Y-doped (2 and 4%) MoO_3 nanorods against MDR *E. coli* have been examined by utilizing the agar well diffusion method, and zone of inhibitions was measured as represented in Table 1. MoO_3 nanorods revealed a lower zone area compared to doped samples against MDR *E. coli.* MoO_3 and Y (2 and 4%) doped samples demonstrated the inhibition zones at (0.5 mg/50 μL) and (1.0 mg/50 μL) doses as (2.65 mm, 2.35 mm, and 3.45 mm) and (4.05 mm, 4.75 mm, and 5.20 mm) correspondingly. The positive control in the inhibition zones MDR *E.coli* (5 mm) was ciprofloxacin as compared to DI (0 mm) water, which was employed as a negative control.

Reactive oxygen species (ROS) are produced by the manufactured MoO_3 and Y-doped MoO_3 nanorods during incubation in the existence of light, as shown in Fig. 8. Particle size, shape, and surface area of produced product have all been found to influence oxidative stress tolerance, and small-size NPs with large surfaces have been shown to have antibacterial potential (Navale et al., 2015; Jesudoss et al., 2016). The

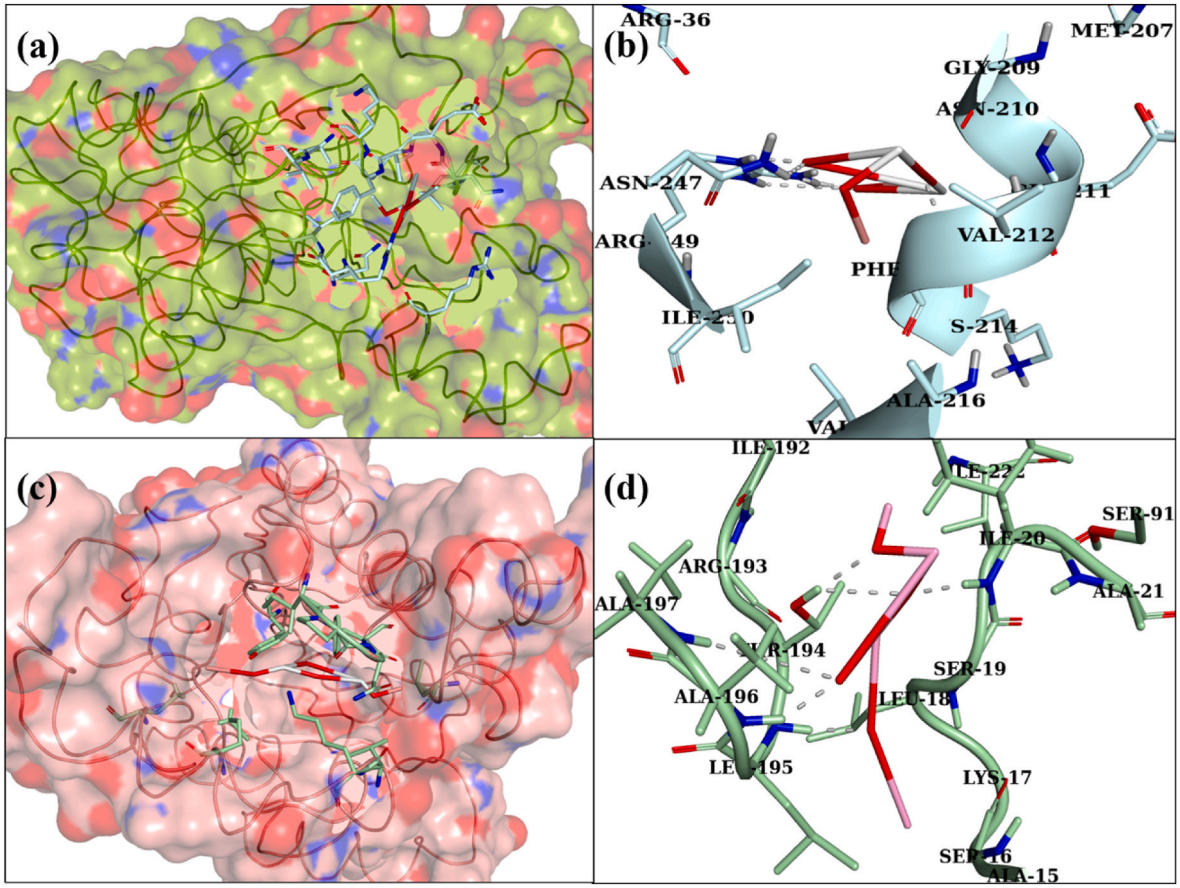

Fig. 9. 3D view of the binding interaction pattern of Y-doped MoO_3 NRs inside the active site of FabH (a, b) and FabI (c,d).

primary unit for ROS generation serves as electron-hole pairs. Increased amounts of ROS like superoxide anion radicals (O^{2-}), hydroxyl radicals (OH^{-}), and hydrogen peroxide radicals (H_2O_2) are produced during the chemical reaction. Under the interaction of the hydrophobic and electrostatic forces, several transition metal oxides are effective against microbes. The extrusion of cytoplasmic content and structure, as well as the eradication of any bacteria found to be able to take responsibility for bacterial cell death, are caused by the electrostatic interaction between these bacterial strains and synthesized materials (Azman et al., 2017; Ahmed et al., 2018, 2019; Ali et al., 2018, 2019). Nanomaterials' biological activities have a long history of research. By interacting with bacterial cells, they may obstruct cell membrane penetration and obliterate important metabolic processes. The precise mechanism underlying the toxicity of nanoparticles to bacteria is still unknown (Rai et al., 2012; Lee et al., 2019).

Numerous studies (Altaf et al., 2020; Arularasu et al., 2020; Ikram et al., 2020) have examined the microbicidal potential of nanoparticles incorporating metal ions. The bioactivity of nanoparticles relies on their capacity to interact with bacteria through electrostatic, van der Waals, or hydrophobic forces (Dakal et al., 2016; Shahzadi et al., 2022). Key targets of antibiotics have been recognized as enzymes belonging to crucial metabolic processes in bacterial cells. Therefore, fatty acid biogenesis enzymes FabI and FabH from *E. coli* were chosen as potential targets to investigate the inhibitory propensity of Y-doped MoO_3 against them.

Fig. 9(c and d) depicts the best-docked conformation of Y-doped MoO_3 within an active pocket of $FabI_{E.\ coli}$, which indicated an H-bond interaction with Ile20, Thr194, Ala196, and Ala197 with overall binding score of 4.96. While for $FabH_{E.\ Coli}$, the major binding interactions were with Phe213, Asn247, and Arg249, and a binding score of 3.66 as presented in (Fig. 9(a and b)).

4. Conclusion

In this study, molybdenum trioxide (MoO_3) and yttrium (Y) doped (2 and 4 wt %) MoO_3 nanorods were fabricated by facile co-precipitation technique. XRD confirmed the multiple crystalline structures of prepared samples as hexagonal, orthorhombic, and monoclinic of pure MoO_3 and upon Y doping, the crystallinity decreased. UV–visible spectroscopy unveiled a red shift in absorption spectra manifested to decrease in Eg from 3.87 to 3.79 eV. PL patterns examined the recombination rate of charge carriers as electrons (e^{-}) and holes (h^{+}). A significant CA was observed against MB dye in an acidic medium at 99.74%, in neutral medium at 92.38%, and in basic medium at 97.87% and efficient bactericidal actions was studied against (*E. coli)* as inhibition zone area of (5.20 mm) for 4% Y-doped MoO_3 at higher concentration. In silico studies suggested Y-doped MoO_3 nanorods as possible inhibitors of FabH and FabI enzymes. In short, MoO_3 nanorods with rare earth metal doped could be efficient against MDR *E.coli* and industrial dye degrader.

Declaration of competing interest

The authors declare that they have no known competing financial interests or personal relationships that could have appeared to influence the work reported in this paper.

Data availability

Data will be made available on request.

Acknowledgment

This research was funded by the Princess Nourah bint Abdulrahman University Researchers Supporting Project number (PNURSP2023R1), Princess Nourah bint Abdulrahman University, Riyadh, Saudi Arabia. Walid Nabgan is grateful for the support from Universitat Rovira i Virgili under the Maria Zambrano Programme (Reference number: 2021URV-MZ-10). Muhammad Ikram is thankful to the higher education commission, Pakistan for financial support through NRPU 20-17615.

Appendix A. Supplementary data

Supplementary data to this article can be found online at https://doi.org/10.1016/j.chemosphere.2023.139855.

References

Adzitey, F., Yussif, S., Ayamga, R., Zuberu, S., Addy, F., Adu-Bonsu, G., Huda, N., Kobun, R., 2022. Antimicrobial susceptibility and molecular characterization of Escherichia coli recovered from milk and related samples. Microorganisms 10, 1335.
Ahmed, B., Hashmi, A., Khan, M.S., Musarrat, J., 2018. ROS mediated destruction of cell membrane, growth and biofilms of human bacterial pathogens by stable metallic AgNPs functionalized from bell pepper extract and quercetin. Adv. Powder Technol. 29, 1601–1616.
Ahmed, B., Solanki, B., Zaidi, A., Khan, M.S., Musarrat, J., 2019. Bacterial toxicity of biomimetic green zinc oxide nanoantibiotic: insights into ZnONP uptake and nanocolloid–bacteria interface. Toxicol. Res. 8, 246–261.
Al-Otaibi, A.L., 2021. Yttrium doped single-crystalline orthorhombic molybdenum oxide micro-belts: synthesis, structural, optical and photocatalytic properties. J. Inorg. Organomet. Polym. Mater. 31, 3416–3429.
Ali, K., Ahmed, B., Ansari, S.M., Saquib, Q., Al-Khedhairy, A.A., Dwivedi, S., Alshaeri, M., Khan, M.S., Musarrat, J., 2019. Comparative in situ ROS mediated killing of bacteria with bulk analogue, Eucalyptus leaf extract (ELE)-capped and bare surface copper oxide nanoparticles. Mater. Sci. Eng. C 100, 747–758.
Ali, K., Ahmed, B., Khan, M.S., Musarrat, J., 2018. Differential surface contact killing of pristine and low EPS Pseudomonas aeruginosa with Aloe vera capped hematite (α-Fe2O3) nanoparticles. J. Photochem. Photobiol. B Biol. 188, 146–158.
Ali, M., Sharif, S., Anjum, S., Imran, M., Ikram, M., Naz, M., Ali, S., 2020. Preparation of Co and Ni doped ZnO nanoparticles served as encouraging nano-catalytic application. Mater. Res. Express 6, 1250d1255.
Altaf, S., Haider, A., Naz, S., Ul-Hamid, A., Haider, J., Imran, M., Shahzadi, A., Naz, M., Ajaz, H., Ikram, M., 2020. Comparative study of selenides and tellurides of transition metals (Nb and Ta) with respect to its catalytic, antimicrobial, and molecular docking performance. Nanoscale Res. Lett. 15, 1–16.
Areerob, Y., Cho, J.Y., Jang, W.K., Oh, W.-C., 2018. Enhanced sonocatalytic degradation of organic dyes from aqueous solutions by novel synthesis of mesoporous Fe3O4-graphene/ZnO@ SiO2 nanocomposites. Ultrason. Sonochem. 41, 267–278.
Arularasu, M., Harb, M., Sundaram, R., 2020. Synthesis and characterization of cellulose/TiO2 nanocomposite: evaluation of in vitro antibacterial and in silico molecular docking studies. Carbohydr. Polym. 249, 116868.
Azman, A.-S., Othman, I., Fang, C.-M., Chan, K.-G., Goh, B.-H., Lee, L.-H., 2017. Antibacterial, anticancer and neuroprotective activities of rare Actinobacteria from mangrove forest soils. Indian J. Microbiol. 57, 177–187.
Bauer, A.W., Kirby, W.M., Sherris, J.C., Turck, M., 1966. Antibiotic susceptibility testing by a standardized single disk method. Am. J. Clin. Pathol. 45, 493–496.
Bergey, D.H., 1994. Bergey's Manual of Determinative Bacteriology. Lippincott Williams & Wilkins.
Bhargava, R., Khan, S., 2017. Effect of reduced graphene oxide (rGO) on structural, optical, and dielectric properties of Mg(OH)2/rGO nanocomposites. Adv. Powder Technol. 28, 2812–2819.
Calderón, D.J., DeAlba-Montero, I., Ruiz, F., Echeverría, F., 2020. Effect of synthesis variables on the characteristics of magnesium hydroxide nanoparticles and evaluation of the fluorescence of functionalised Mg (OH) 2 nanoparticles. Adv. Nat. Sci. Nanosci. Nanotechnol. 11, 025008.
Chahal, S., Rani, N., Kumar, A., Kumar, P., 2019. UV-irradiated photocatalytic performance of yttrium doped ceria for hazardous Rose Bengal dye. Appl. Surf. Sci. 493, 87–93.
Clinical, Institute, L.S., 2017. Performance Standards for Antimicrobial Susceptibility Testing. Clinical and Laboratory Standards Institute Wayne, PA.
Dakal, T.C., Kumar, A., Majumdar, R.S., Yadav, V., 2016. Mechanistic basis of antimicrobial actions of silver nanoparticles. Front. Microbiol. 7, 1831.
Desai, N., Mali, S., Kondalkar, V., Mane, R., Hong, C., Bhosale, P., 2015. Chemically grown MoO3 nanorods for antibacterial activity study. J. Nanomed. Nanotechnol. 6, 1.
Dewangan, K., Singh, D., Satpute, N., Singh, R., Jaiswal, A., Shrivas, K., Bahadur, I., 2022. Hydrothermally grown α-MoO3 microfibers for photocatalytic degradation of methylene blue dye. J. Mol. Liq. 349, 118202.
Din, M.I., Khalid, R., Najeeb, J., Hussain, Z., 2021. Fundamentals and photocatalysis of methylene blue dye using various nanocatalytic assemblies-a critical review. J. Clean. Prod. 298, 126567.
Donnadieu, A., Davazoglou, D., Abdellaoui, A., 1988. Structure, optical and electro-optical properties of polycrystalline WO3 and MoO3 thin films prepared by chemical vapour deposition. Thin Solid Films 164, 333–338.
Gautam, S., Agrawal, H., Thakur, M., Akbari, A., Sharda, H., Kaur, R., Amini, M., 2020. Metal oxides and metal organic frameworks for the photocatalytic degradation: a review. J. Environ. Chem. Eng. 8, 103726.

Gowtham, B., Ponnuswamy, V., Pradeesh, G., Chandrasekaran, J., Aradhana, D., 2018. MoO3 overview: hexagonal plate-like MoO3 nanoparticles prepared by precipitation method. J. Mater. Sci. Mater. Electron. 29, 6835–6843.
Gupta, V.K., Kumar, R., Nayak, A., Saleh, T.A., Barakat, M., 2013. Adsorptive removal of dyes from aqueous solution onto carbon nanotubes: a review. Adv. Colloid Interface Sci. 193, 24–34.
Haider, A., Ijaz, M., Ali, S., Haider, J., Imran, M., Majeed, H., Shahzadi, I., Ali, M.M., Khan, J.A., Ikram, M., 2020a. Green synthesized phytochemically (zingiber officinale and allium sativum) reduced nickel oxide nanoparticles confirmed bactericidal and catalytic potential. Nanoscale Res. Lett. 15, 50.
Haider, A., Ijaz, M., Imran, M., Naz, M., Majeed, H., Khan, J., Ali, M., Ikram, M., 2020b. Enhanced bactericidal action and dye degradation of spicy roots' extract-incorporated fine-tuned metal oxide nanoparticles. Appl. Nanosci. 10, 1095–1104.
Hassan, J., Ikram, M., Ul-Hamid, A., Imran, M., Aqeel, M., Ali, S., 2020. Application of chemically exfoliated boron nitride nanosheets doped with Co to remove organic pollutants rapidly from textile water. Nanoscale Res. Lett. 15, 75.
He, X., Hou, J., Sun, X., Jangili, P., An, J., Qian, Y., Kim, J., Shen, J., NIR-II, P.-A.S.T., 2022. Using sodium molybdenum bronze nanoplatform against subcutaneous Staphylococcus aureus infection. Adv. Funct. Mater. 32, 2203964.
He, X., Qian, Y., Wu, C., Feng, J., Sun, X., Zheng, Q., Li, X., Shen, J., 2023. Entropy-Mediated high-entropy MXenes nanotherapeutics: NIR-II-Enhanced intrinsic oxidase mimic activity to combat methicillin-resistant Staphylococcus aureus infection. Adv. Mater., 2211432
Hussain, M.K., Khalid, N., 2022a. Surfactant-assisted synthesis of MoO3 nanorods and its application in photocatalytic degradation of different dyes in aqueous environment. J. Mol. Liq. 346, 117871.
Hussain, M.K., Khalid, N.R., 2022b. Surfactant-assisted synthesis of MoO3 nanorods and its application in photocatalytic degradation of different dyes in aqueous environment. J. Mol. Liq. 346, 117871.
Ikram, M., Hassan, J., Raza, A., Haider, A., Naz, S., Ul-Hamid, A., Haider, J., Shahzadi, I., Qamar, U., Ali, S., 2020. Photocatalytic and bactericidal properties and molecular docking analysis of TiO 2 nanoparticles conjugated with Zr for environmental remediation. RSC Adv. 10, 30007–30024.
Ikram, M., Inayat, T., Haider, A., Ul-Hamid, A., Haider, J., Nabgan, W., Saeed, A., Shahbaz, A., Hayat, S., Ul-Ain, K., Butt, A.R., 2021. Graphene oxide-doped MgO nanostructures for highly efficient dye degradation and bactericidal action. Nanoscale Res. Lett. 16, 56.
Irmawati, R., Shafizah, M., 2009. The production of high purity hexagonal MoO3 through the acid washing of as-prepared solids. Int. J. Basic Appl. Sci. 9, 241–244.
Iwalokun, B., Ogunledun, A., Ogbolu, D., Bamiro, S., Jimi-Omojola, J., 2004. In vitro antimicrobial properties of aqueous garlic extract against multidrug-resistant bacteria and Candida species from Nigeria. J. Med. Food 7, 327–333.
Jesudoss, S.K., Vijaya, J.J., Kennedy, L.J., Rajan, P.I., Al-Lohedan, H.A., Ramalingam, R. J., Kaviyarasu, K., Bououdina, M., 2016. Studies on the efficient dual performance of Mn1–xNixFe2O4 spinel nanoparticles in photodegradation and antibacterial activity. J. Photochem. Photobiol. B Biol. 165, 121–132.
Kandasamy, B., Govindasamy, P., Thangavelu, P., Theerthagiri, J., Min, A., Choi, M.Y., 2022. Improved visible light photocatalytic degradation of yttrium doped NiMgAl layered triple hydroxides for the effective removal of methylene blue dye. Chemosphere 290, 133299.
Klinbumrung, A., Thongtem, T., Thongtem, S., 2012. Characterization of orthorhombic α-MoO3 microplates produced by a microwave plasma process. J. Nanomater. 2012 (930763) 2012.
Krishnamoorthy, K., Veerapandian, M., Yun, K., Kim, S.J., 2013. New function of molybdenum trioxide nanoplates: toxicity towards pathogenic bacteria through membrane stress. Colloids Surf. B Biointerfaces 112, 521–524.
Lee, N., Ko, W., Hsueh, P., 2019. Nanoparticles in the treatment of infections caused by multidrug-resistant organisms. Front. Pharmacol. 10, 1153.
Lippincott, E.R., 1963. Infrared spectra of inorganic and coordination compounds. J. Am. Chem. Soc. 85, 3532-3532.
M, K.K., K, B., G, N., B, S., A, V., 2016. Plasmonic resonance nature of Ag-Cu/TiO2 photocatalyst under solar and artificial light: synthesis, characterization and evaluation of H2O splitting activity. Appl. Catal. B Environ. 199, 282–291.
Magaldi, S., Mata-Essayag, S., De Capriles, C.H., Pérez, C., Colella, M., Olaizola, C., Ontiveros, Y., 2004. Well diffusion for antifungal susceptibility testing. Int. J. Infect. Dis. 8, 39–45.
McKinney, D.C., Eyermann, C.J., Gu, R.-F., Hu, J., Kazmirski, S.L., Lahiri, S.D., McKenzie, A.R., Shapiro, A.B., Breault, G., 2016. Antibacterial FabH inhibitors with mode of action validated in Haemophilus influenzae by in vitro resistance mutation mapping. ACS Infect. Dis. 2, 456–464.
Mehmood, Z., Ikram, M., Imran, M., Shahzadi, A., Haider, A., Ul-Hamid, A., Nabgan, W., Haider, J., Hayat, S., 2022. Z. officinale-doped silver/calcium oxide nanocomposites: catalytic activity and antimicrobial potential with molecular docking analysis. Process Biochem. 121, 635–646.
Naik, S.S., Lee, S.J., Begildayeva, T., Yu, Y., Lee, H., Choi, M.Y., 2020. Pulsed laser synthesis of reduced graphene oxide supported ZnO/Au nanostructures in liquid with enhanced solar light photocatalytic activity. Environ. Pollut. 266, 115247.
Navale, G.R., Rout, C.S., Gohil, K.N., Dharne, M.S., Late, D.J., Shinde, S.S., 2015. Oxidative and membrane stress-mediated antibacterial activity of WS2 and rGO-WS2 nanosheets. RSC Adv. 5, 74726–74733.
Naz, M., Rafiq, A., Ikram, M., Haider, A., Ahmad, S.O.A., Haider, J., Naz, S., 2021. Elimination of dyes by catalytic reduction in the absence of light: a review. J. Mater. Sci. 56, 15572–15608.
Parangusan, H., Ponnamma, D., Al-Maadeed, M.A.A., Marimuthu, A., 2018. Nanoflower-like yttrium-doped ZnO photocatalyst for the degradation of methylene blue dye. Photochem. Photobiol. 94, 237–246.
Qumar, U., Ikram, M., Imran, M., Haider, A., Ul-Hamid, A., Haider, J., Riaz, K.N., Ali, S., 2020. Synergistic effect of Bi-doped exfoliated MoS2 nanosheets on their bactericidal and dye degradation potential. Dalton Trans. 49, 5362–5377.
Rafiq, A., Ikram, M., Ali, S., Niaz, F., Khan, M., Khan, Q., Maqbool, M., 2021. Photocatalytic degradation of dyes using semiconductor photocatalysts to clean industrial water pollution. J. Ind. Eng. Chem. 97, 111–128.
Rai, M.K., Deshmukh, S., Ingle, A., Gade, A., 2012. Silver nanoparticles: the powerful nanoweapon against multidrug-resistant bacteria. J. Appl. Microbiol. 112, 841–852.
Raj, A.N.P., Bennie, R.B., Joel, C., Kengaram, S.H., Abraham, S.D., 2022. Systematic analysis and the effect of Mn doping on structural, optical and magnetic properties of MoO3 nanoparticles. Solid State Commun. 341, 114532.
Rajiv Chandar, N., Agilan, S., Thangarasu, R., Muthukumarasamy, N., Chandrasekaran, J., Arunachalam, S., Akshaya, S., 2021. Elucidation of efficient dual performance in photodegradation and antibacterial activity by a promising candidate Ni-doped MoO3 nanostructure. J. Sol. Gel Sci. Technol. 100, 451–465.
Ramu, A., Salla, S., Chandrasekaran, S., Silambarasan, P., Gopi, S., Seo, S.-y., Yun, K., Choi, D., 2021. A facile synthesis of metal ferrites and their catalytic removal of toxic nitro-organic pollutants. Environ. Pollut. 270, 116063.
Raza, A., Hassan, J., Ikram, M., Naz, S., Haider, A., Ul-Hamid, A., Shahzadi, I., Haider, J., Goumri-Said, S., Kanoun, M., 2021. Molecular docking and DFT analyses of magnetic cobalt doped MoS2 and BN nanocomposites for catalytic and antimicrobial explorations. Surface. Interfac. 27, 101571.
Savage, N., Diallo, M.S., 2005. Nanomaterials and water purification: opportunities and challenges. J. Nanoparticle Res. 7, 331–342.
Seefeld, M.A., Miller, W.H., Newlander, K.A., Burgess, W.J., DeWolf, W.E., Elkins, P.A., Head, M.S., Jakas, D.R., Janson, C.A., Keller, P.M., 2003. Indole naphthyridinones as inhibitors of bacterial enoyl-ACP reductases FabI and FabK. J. Med. Chem. 46, 1627–1635.
Sen, S.K., Dutta, S., Khan, M., Manir, M., Dutta, S., Al Mortuza, A., Razia, S., Hakim, M., 2019. Characterization and antibacterial activity study of hydrothermally synthesized h-MoO3 nanorods and α-MoO3 nanoplates. BioNanoScience 9, 873–882.
Senthilkumar, R., Anandhababu, G., Mahalingam, T., Ravi, G., 2016. Photoelectrochemical study of MoO3 assorted morphology films formed by thermal evaporation. J. Energy Chem. 25, 798–804.
Shaban, M., Ashraf, A.M., Abukhadra, M.R., 2018. TiO2 nanoribbons/carbon nanotubes composite with enhanced photocatalytic activity; fabrication, characterization, and application. Sci. Rep. 8, 1–17.
Shahzadi, I., Islam, M., Saeed, H., Haider, A., Shahzadi, A., Haider, J., Ahmed, N., Ul-Hamid, A., Nabgan, W., Ikram, M., 2022. Formation of biocompatible MgO/cellulose grafted hydrogel for efficient bactericidal and controlled release of doxorubicin. Int. J. Biol. Macromol. 220, 1277–1286.
Sharma, P.K., Raghubanshi, A., Shah, K., 2020. Examining dye degradation and antibacterial properties of organically induced α-MoO3 nanoparticles, their uptake and phytotoxicity in rice seedlings. Environ. Nanotechnol. Monit. Manag. 14, 100315.
Sharma, R., Sarkar, A., Jha, R., Sharma, A.K., Bhushan, M., Bhardwaj, R., 2022. Synthesis & material properties of α-MoO3 nanoparticles. Mater. Today: Proc. 48, 683–686.
Siriwong, C., Wetchakun, N., Inceesungvorn, B., Channei, D., Samerjai, T., Phanichphant, S., 2012. Doped-metal oxide nanoparticles for use as photocatalysts. Prog. Cryst. Growth Char. Mater. 58, 145–163.
Taghizadeh, M.T., Siyahi, V., Ashassi-Sorkhabi, H., Zarrini, G., 2020. ZnO, AgCl and AgCl/ZnO nanocomposites incorporated chitosan in the form of hydrogel beads for photocatalytic degradation of MB, E. coli and S. aureus. Int. J. Biol. Macromol. 147, 1018–1028.
Valgas, C., Souza, S.M.d., Smânia, E.F., Smânia Jr., A., 2007. Screening methods to determine antibacterial activity of natural products. Braz. J. Microbiol. 38, 369–380.
Vamathevan, V., Amal, R., Beydoun, D., Low, G., McEvoy, S., 2002. Photocatalytic oxidation of organics in water using pure and silver-modified titanium dioxide particles. J. Photochem. Photobiol. Chem. 148, 233–245.
Yogananda, H.S., Nagabhushana, H., Naik, R., Prashantha, S.C., 2018. Calcination temperature dependent structural modifications, tailored morphology and luminescence properties of MoO3 nanostructures prepared by sonochemical method. J. Sci.: Adv. Mater. Dev. 3, 77–85.
Zakharova, G., Täschner, C., Volkov, V., Hellmann, I., Klingeler, R., Leonhardt, A., Büchner, B., 2007. MoO3− δ nanorods: synthesis, characterization and magnetic properties. Solid State Sci. 9, 1028–1032.